TECHNICAL TRANSACTIONS | CZASOPISMO TECHNICZNE
CIVIL ENGINEERING | BUDOWNICTWO
6-B/2014

MICHAŁ PAZDANOWSKI*

RESIDUAL STRESS DEVELOPMENT IN RAILROAD RAILS – A PARAMETRIC STUDY

STUDIUM PARAMETRYCZNE NAPRĘŻEŃ RESZTKOWYCH W SZYNIE KOLEJOWEJ

Abstract

This paper presents the results of a parametric study undertaken to analyse the influence that changes in the material model and contact zone parameters may have on residual stress levels. A simplified shakedown based mechanical model is used to estimate the residual stress distributions due to simulated contact loads. An information on final shakedown state of the rail subjected to given loading program is obtained at a substantially reduced computational cost compared to the standard incremental analysis. A 50% increase in peak contact pressure may increase the longitudinal residual stress level by over 700%. The dependence of peak residual stresses on changes in the hardening ratio is almost linear, while the dependence of peak residual stresses on changes in the yield limit indicates a quadratic relationship. The research indicates that in future applications, a simplified treatment of the rail/wheel interface is justified, as long as the peak pressure in the contact zone is estimated correctly. The residual stresses in rails induced by service conditions may reach very high values, on a par with the material yield limit. This effect is aggravated by the operating procedure of increasing wheel axle loads.

Keywords: *residual stresses*, *numerical techniques*, *material properties*

Streszczenie

W niniejszym opracowaniu przedstawiono wyniki studium parametrycznego przeprowadzonego w celu zbadania wpływu zmian modelu materiału i parametrów strefy kontaktu na poziom naprężeń resztkowych w szynie kolejowej. Uproszczony model mechaniczny, oparty na teorii plastycznego przystosowania, został zastosowany do oszacowania rozkładu naprężeń resztkowych wywołanych symulowanymi obciążeniami kontaktowymi. Stwierdzono, że 50% wzrost maksymalnego ciśnienia w strefie kontaktu skutkuje wzrostem maksymalnych naprężeń resztkowych o około 700%, przy czym zależność maksymalnych naprężeń resztkowych od zmian współczynnika wzmocnienia materiału szyny ma charakter liniowy, podczas gdy zależność tych samych naprężeń od wartości granicy plastyczności ma charakter kwadratowy. Przeprowadzone obliczenia wskazują, że uproszczone traktowanie strefy kontaktu koło/szyna jest uzasadnione, jak długo maksymalne wartości ciśnienia w tej strefie są oszacowane poprawnie. Naprężenia resztkowe w szynie kolejowej, wywołane przez obciążenia eksploatacyjne kołami taboru, mogą osiągnąć bardzo duże wartości, porównywalne z wartością granicy plastyczności materiału. Efekt ten pogłębia się na skutek zwiększania obciążeń na oś taboru.

Słowa kluczowe: *analiza i modelowanie*, *naprężenia resztkowe*, *metody numeryczne*, *własności materiału*

* Ph.D. Michał Pazdanowski, Institute for Computational Civil Engineering, Faculty of Civil Engineering, Cracow University of Technology.

1. Introduction

Rail breakages may be counted among the important factors negatively affecting the safety of railroad operations. Although this does not usually lead to extreme consequences, unfavourable conditions may result in the catastrophic failure of a section of rail, followed by derailment, loss of life and substantial damage to property [25, 27]. Research [24] shows, that there is a long term growing trend behind this phenomenon, due to heavier axial loads, increased volumes of traffic and longitudinal tensile stresses in low temperatures in continuously welded rails. The economic costs of rail fracture in European Union alone are estimated at €200 million [1].

Research [11] indicates that the rail failure is at least in part to blame on excessive residual stress levels in rails [6, 9, 23] attained during manufacture and service life. Therefore, an effort has been undertaken to estimate the residual stress levels induced in the railroad rail during manufacturing (heat treatment and subsequent straightening) as well as service using both experimental [10, 11, 28] and numerical [20, 22] approaches. Since a traditional elastic-plastic incremental analysis of multiple rolling contacts during service is very time consuming [4], a simplified model of residual stress calculation based on shake-down and Melan's [12] theorem was proposed, first for elastic-perfectly plastic material model [14], and later on, extended for elastic-plastic material exhibiting hardening [2, 17].

The research reported in this paper deals with the application of these basic and extended material models to estimate the changes in residual stress levels in railroad rails due to variations in certain parameters of the rail/wheel contact interface as well as material properties (yield limit and hardening ratio). The results of calculations may yield valuable insights regarding the influence that the deterioration of rail material properties exerts on residual stresses in the rail head.

2. Mechanical model

The mechanical model developed to deal with residual stresses emerging as a result of repetitive contact loads in elastic-plastic material exhibiting kinematic hardening may be presented as the following two step:

I compute the correlation matrix A_{ijkl}:

$$\sigma_{ij}^{r} = A_{ijkl}\ \varepsilon_{kl}^{p} \tag{1}$$

solving the following nonlinear constrained optimization problem for self-equilibrated stresses σ_{ij}^{r} as a function of plastic distortions ε_{ij}^{p}:

$$\min_{\varepsilon_{ij}^{p}} \Theta\left(\sigma_{ij}^{r}\right),\ \ \Theta\left(\sigma_{ij}^{r}\right) = \int_{V} \sigma_{ij}^{r}\ C_{ijkl}\ \sigma_{kl}^{r}\ dV - \int_{V} \varepsilon_{ij}^{p}\ \sigma_{ij}^{r}\ dV \tag{2}$$

at:

$$\sigma^{r}_{ij,j} = 0, \qquad \text{in } V - \text{internal equilibrium conditions,} \tag{3}$$

$$\sigma^{r}_{ij}\ n_j = 0, \qquad \text{on } \partial V - \text{static boundary conditions,} \tag{4}$$

II find plastic distortions ε^{p}_{ij}, minimizing the total complementary energy functional:

$$\min_{\varepsilon^{p}_{ij}} \Psi\left(\varepsilon^{p}_{ij}\right), \quad \Psi\left(\varepsilon^{p}_{ij}\right) = \int_{V} \varepsilon^{p}_{gh}\ A^{T}_{ghij}\ C_{ijkl}\ A_{klmn}\ \varepsilon^{p}_{mn}\ dV \tag{5}$$

at:

$$\Phi\left(A_{ijkl}\ \varepsilon^{p}_{kl} + c\ \varepsilon^{pc}_{ij} + \sigma^{E}_{ij} + \sigma^{t}_{ij}\right) - 1 \le 0, \text{ in } V - \text{yield conditions,} \tag{6}$$

where:

$$c = \frac{E \cdot H}{E - H} \quad - \text{kinematic hardening parameter.}$$

The following denotations hold in formulas (1) through to (6):

- σ^{r}_{ij} – residual stresses induced in the body by the applied cyclic loading program,
- ε^{p}_{ij} – plastic distortions,
- ε^{pc}_{ij} – plastic distortions assumed to have constant spatial distribution during iteration,
- σ^{E}_{ij} – elastic stresses (calculated as if the body deformed purely elastically during the considered cyclic loading program),
- σ^{t}_{ij} – thermal stresses (calculated as if the body deformed purely elastically during the service induced heating),
- A_{ghij} – correlation matrix linking plastic distortions and residual stresses,
- C_{ijkl} – elastic compliance matrix,
- E – Young modulus,
- H – elastic plastic tangent modulus.

In order to ensure the convergence of computer routines, plastic distortions have to be determined using the iterative approach:

$$^{n}\varepsilon^{pc}_{ij} = \lambda\ {}^{n-1}\varepsilon^{pc}_{ij} + (1-\lambda)\ {}^{n-2}\varepsilon^{pc}_{ij}, \ \lambda \in (0,1), \tag{7}$$

where, during iteration 1 initial plastic distortions $^{0}\varepsilon^{pc}_{ij} = 0$, and during subsequent iterations the above formula (7) is used to determine the current levels of plastic distortions. Numerical tests have shown [18] that such an iterative procedure is convergent, and while any value of λ belonging to the interval (0, 1) may be used, $\lambda = 0.5$ led to the final, stable spatial distribution of plastic distortions in the lowest number of iterations. This number of iterations never exceeded 19, though numerical solutions of sufficient quality have been obtained in as few as 7 iterations [18].

3. Numerical procedure

The mechanical problem delineated in (2)–(6) may be analyzed using any discrete method (such as Boundary Element [29], Finite Element [3], or Finite Difference [5]). For the purpose of this research, the Finite Difference Method (FDM) generalized for arbitrary irregular grids [7, 8, 13] has been used to solve the problem on a set of nodes distributed in a cross-section. In order to develop the necessary approximation formulas for functions and their first derivatives at discrete locations, a local coordinate system is introduced at such points of interest (Fig. 1). Then the unknown function is expanded into a Taylor series with respect to neighbouring nodes:

$$f_j = f_0 + h_j \cdot \frac{\partial f_0}{\partial x} + k_j \cdot \frac{\partial f_0}{\partial y} + \frac{h_j^2}{2} \cdot \frac{\partial^2 f_0}{\partial x^2} + h_j \cdot k_j \cdot \frac{\partial^2 f_0}{\partial x \partial y} + \frac{k_j^2}{2} \cdot \frac{\partial^2 f_0}{\partial y^2} + O\left(r^3\right) = \tilde{f}_j + O\left(r^3\right) \quad (8)$$

where:

$$h_j = x_j - x_0, \quad k_j = y_j - y_0, \quad (9)$$

$$r_j = \sqrt{h_j^2 + k_j^2} \quad (10)$$

f_j – value of the function $f = f(x, y)$ at the node j adjacent to the point of interest,
f_0 – value of the function f at the point of interest, i.e. $f_0 = f(x_0, y_0)$.

A weighted minimization method is subsequently applied in order to find a local approximation of the unknown function $f(x, y)$ by a surface of the requested order. In the case of the second order surface, the following weighted error functional is built:

$$B = \sum_{j=1}^{n} \left[\left(-f_j + f_0 + h_j \cdot \frac{\partial f_0}{\partial x} + k_j \cdot \frac{\partial f_0}{\partial y} + \frac{h_j^2}{2} \cdot \frac{\partial^2 f_0}{\partial x^2} + h_j \cdot k_j \cdot \frac{\partial^2 f_0}{\partial x \partial y} + \frac{k_j^2}{2} \cdot \frac{\partial^2 f_0}{\partial y^2} \right) \cdot \frac{1}{r^{p+1}} \right]^2 \quad (11)$$

where j enumerates all the nodes adjacent to the point of interest, p denotes the truncation level of the Taylor series, and at the same time order of the approximating surface. B is minimized with respect to the unknown function f and its derivatives at the point of interest (x_0, y_0). In this manner, a set of linear equations is generated which is later solved for the unknown finite difference coefficients of function and its derivatives at the point of interest.

This weighted minimization method may be used to compute approximate value of function f or to determine coefficients of finite difference operators. Thus, the function or its derivatives may be approximated at any point, like Gauss stations or equilibrium equations, and yield conditions application points (Fig. 2).

Finally, a variant of the Feasible Directions Method [15], tailored to the quadratic objective function (5) and constraints (6) has been applied to solve the optimization problem (5), (6) for plastic distortions.

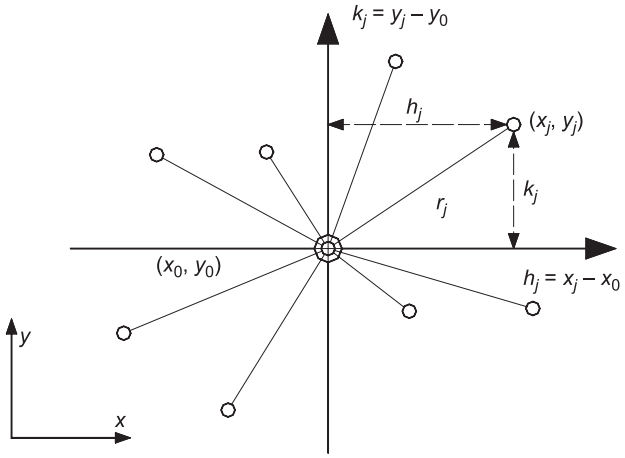

Fig. 1. Irregular set of nodes for finite difference operator

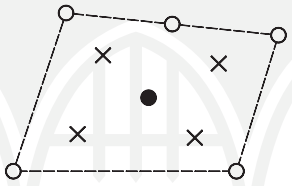

Fig. 2. Approximation and integration between nodes: ○ – nodes *j*, ✕ – Gauss stations, ● – equilibrium equations and yield condition application point

4. Parametric studies

The following material data have been used for comparative calculations:

Rail	132RE
Young modulus	E = 206 GPa
Yield limit	Y = 480 MPa
Poisson's ratio	v = 0,3
Track foundation modulus	kv = 20.6 MPa
Static wheel load	P = 120, 134, 147, 160, 178 kN

These have been chosen to realistically represent the conditions existing on heavy haul revenue railroads [23]. The following studies have been undertaken to examine the dependence of residual stresses in the railroad rail on certain parameters of the contact interface: pressure distribution in the contact zone, changes in the yield limit, changes in the hardening ratio.

The standard approach of the operating procedure used to determine pressure distribution in the wheel/rail interface on North American railroads [16] is to calculate the contact area

using standard elastic Hertz formulae for two curved bodies in contact, then to find a rectangle of an equivalent area and having a ratio of c_z/c_x = 1.6 (c_z is aligned with the longitudinal axis of rail). A biparabolic pressure distribution over such a rectangle has been assumed to be correctly approximating the real one, while the peak pressure p_0 has been computed via the static equivalence requirement of the applied wheel load P and the pressure distribution assumed, leading to the formula:

$$p_0 = \frac{9}{4} \cdot \frac{P}{c_x \cdot c_z} \tag{12}$$

The real rail/wheel interface differs substantially from the standard Hertz contact problem (elastic-plastic rolling contact vs. static elastic contact). This includes the shape of the contact zone as well as the pressure distribution within the contact area [26]. Since no reliable experimental data is available, the parametric study presented here was intended to investigate the influence these two parameters of rail/wheel contact (patch shape and size, peak contact pressure) have on levels of residual stresses in the rail. Four separate pressure distributions spanned over a rectangle (Fig. 3a–c)) and a diamond (Fig. 3d)) were selected as simplified geometrical forms corresponding to the computer simulations of pressure distribution in rail/wheel interface in both elastic [30] and elastic-plastic rolling contact [19]. The analysis was accomplished during three separate tests, applying the loads listed above.

In the first test, a static wheel load of 147 kN was applied to the rail, spanned over the areas depicted in Fig. 3. Based on the results of this test, for the remaining tests a pressure distribution, depicted in Fig. 3a), was used. In the second test, a constant patch size was kept irrespective of the load level, while peak pressure was adjusted to satisfy the equilibrium condition; in the third test, the opposite was true. In all cases, the load was applied at the rail axis of symmetry. Some of the test results are presented in Figs. 4 and 5.

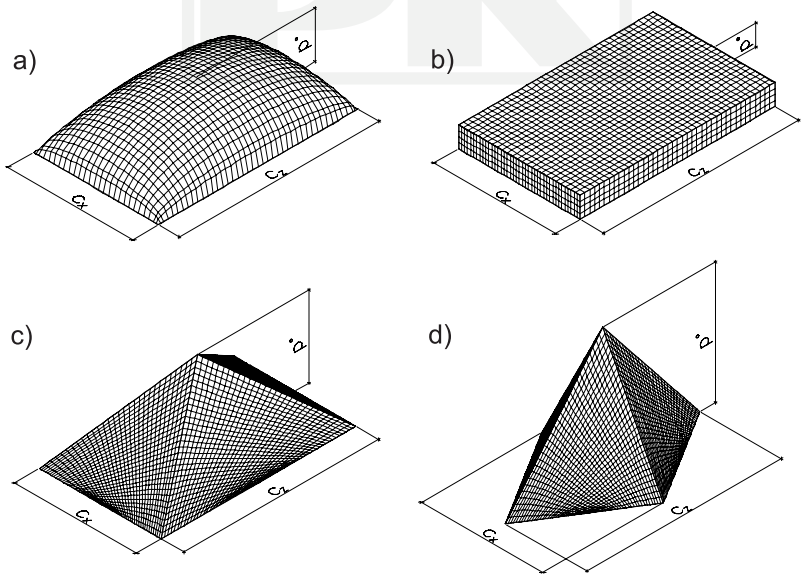

Fig. 3. Pressure distributions used in parametric study

As Figs. 4 and 5 indicate, an increase in peak contact pressure does not affect the location of peak compressive σ_{zz} residual stress, while it does substantially affect the depth of peak tensile σ_{zz} residual stress location, pushing it downwards by about 7 mm. However, if the peak contact pressure is kept constant, both values and locations of peak tensile and compressive σ_{zz} residual stresses remain fairly stable as may be observed in Figs. 5 and 6.

In the following group of tests, the combined effect that the changing yield limit and hardening ratio may exert on the level of residual stresses in the railroad rail has been investigated. The 147 kN load was again applied at the rail crown. The residual stresses have been determined fifteen times, in three groups of five tests in order to cover all possible yield limit/hardening ratio combinations while assuming predetermined ±5% and ±10% fluctuations of the 480 MPa yield limit value and ±10% fluctuations of the assumed hardening ratio c = 1/9 (Figs. 7 and 8).

The results obtained during these calculations seem to indicate that the service induced peak residual stresses exhibit quadratic dependence on the yield limit, irrespective of the hardening ratio assumed, at least within the bounds considered in this study. At the same time, the influence of changes in the hardening ratio on peak residual stresses seems to be negligible within the considered bounds, as may be observed in Fig. 7, where the peak stress evolution curves corresponding to the considered hardening ratios follow each other closely.

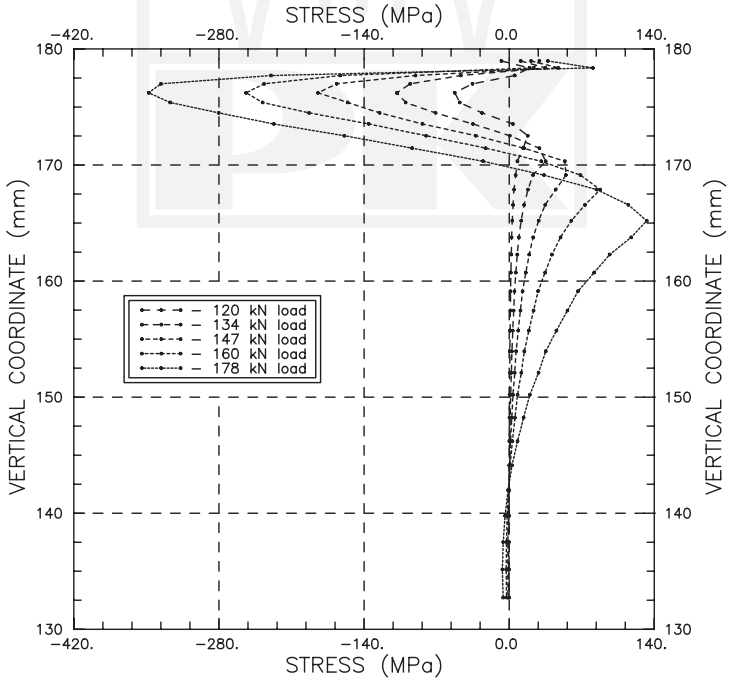

Fig. 4. Longitudinal residual stress along the rail's vertical axis of symmetry vs. the distance from rail foot, constant patch case

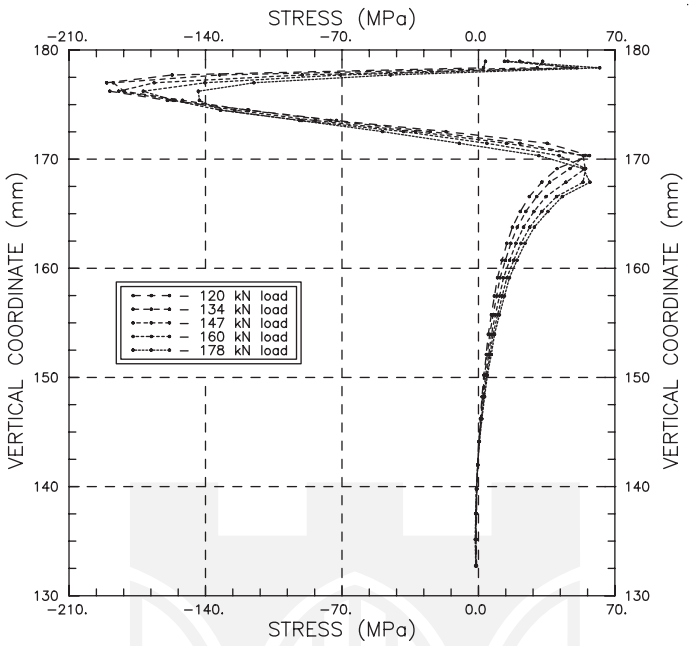

Fig. 5. Longitudinal residual stress along the rail's vertical axis of symmetry vs. the distance from the rail foot, constant peak pressure case

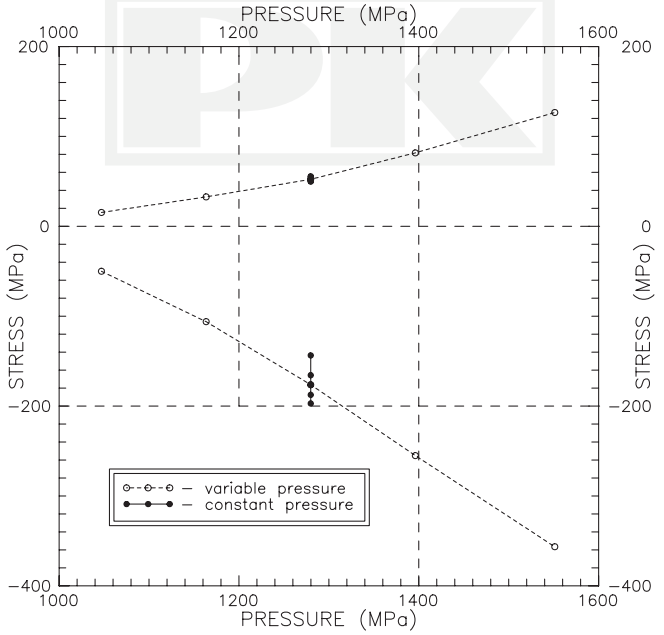

Fig. 6. Peak longitudinal residual stress values in the cross-section vs. peak contact pressure (positive value denotes tension)

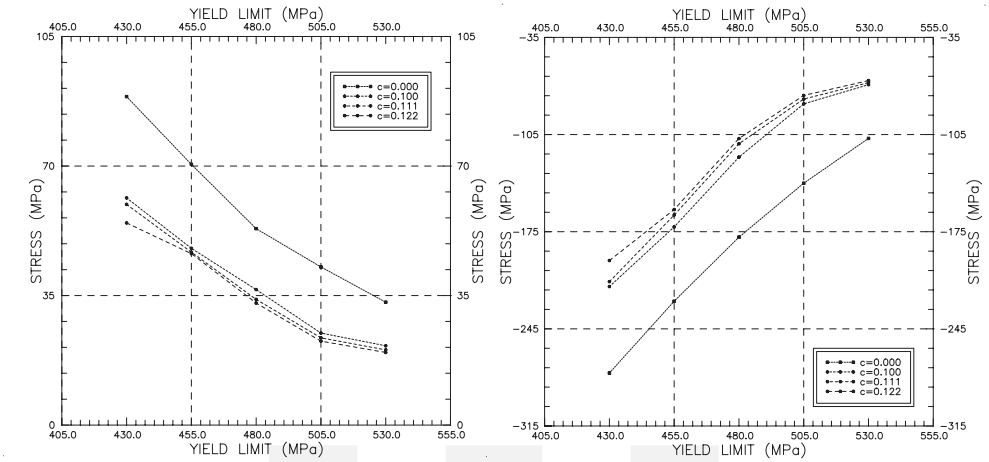

Fig. 7. Peak longitudinal residual stress, vs. yield limit, tension (left) and compression (right); $c = 0.0$ – perfect plasticity

The near-horizontal lines depicting dependence of peak residual stresses on the hardening ratio in Fig. 8 for all analyzed yield limit values corroborate this observation.

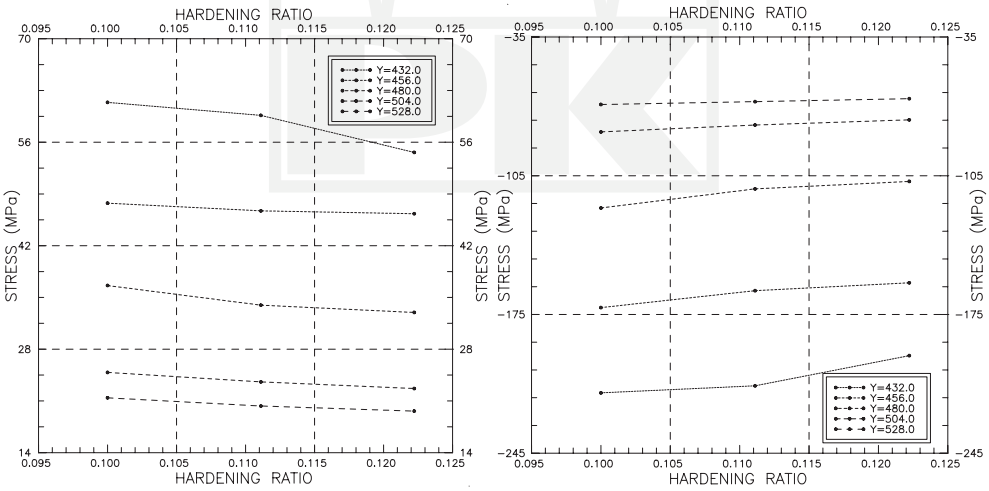

Fig. 8. Peak longitudinal residual stress versus hardening ratio, tension (left) and compression (right); Y – yield limit

Results obtained for all the considered yield limit fluctuations around the reference value of 480 MPa at the hardening ratio of $c = 1/9$, but representative for all the considered yield limit/hardening ratio scenarios, are presented in the Tab. 1. These results indicate that

a 10% decrease in material yield limit results in an approximately 80% increase in peak values of residual stresses with an exception of σ_{yy}, for which this ratio is substantially lower (approximately 30% in compression and 60% in tension), while a 10% increase in material yield limit results in an approximately 40% decrease in respective stress values, again, with an exception of σ_{yy}, for which this ratio is closer to 25%.

Table 1

Relative changes in peak values of residual stress components in rail

LOADING CASE (change in yield limit)	STRESS CHANGE [%]							
	σ_{xx}		σ_{yy}		σ_{zz}		σ_{xy}	
	min.[2)]	max.[2)]	min.[2)]	max.[2)]	min.[2)]	max.[2)]	min.[2)]	max.[2)]
1 (–10%)	74.26	82.29	26.77	62.43	89.03	75.61	72.20	72.20
2 (–5%)	37.60	41.29	13.13	26.93	46.02	37.58	39.14	39.14
3 (0%)[1)]	0.00	0.00	0.00	0.00	0.00	0.00	0.00	0.00
4 (+5%)	–41.48	–32.65	–15.63	–23.23	–28.86	–30.57	–23.77	–23.77
5 (+10%)	–35.98	–41.69	–23.43	–29.31	–39.43	–40.18	–35.69	–35.69

[1)] – a reference solution;
[2)] – min. – compression, max. – tension.

5. Conclusions

The following conclusions have been drawn with respect to the residual stress distributions in railroad rails and peak levels of these stresses based on the test results:

a) the residual stresses are not very sensitive to the shape of the contact zone and the shape of pressure distribution, but peak contact pressure matters;
b) the general distribution of residual stresses (location of compressive and tensile zones and points of peak pressure) is practically immune to changes in the way in which the contact load is applied, as long as the peak pressure remains unchanged;
c) a 50% increase in peak contact pressure may increase the longitudinal residual stress level by over 700% (see Figs. 4 and 6);
d) dependence of peak residual stresses on changes in the hardening ratio is almost linear (with the one exception being the weakest material) within the bounds considered, this dependence is negligible;
e) dependence of peak residual stresses on changes in the yield limit indicates a quadratic relationship, weakening at the highest yield limits; moderate changes in the yield limit result in very substantial changes to peak stress values (an up to 9:1 ratio of the relative stress change to the relative yield limit change is observed for the longitudinal residual stress) (see Tab. 1).

The following further actions are proposed to enhance and improve the presented mechanical/numerical model in order to better approximate the residual stress distributions in the railroad rail subject to service conditions:

a) modelling of wear due to contact phenomena on the rail/wheel interface, or due to maintenance procedures (grinding);
b) inclusion of the residual stress state introduced by the manufacturing process (quenching and roller straightening) in the analysis of residual stresses due to live loads;
c) application of a fuzzy sets theory to estimate the effect that fluctuations in material constants' values and parameters of contact may have on the residual stresses.

Ultimately, knowledge of the full evolution of residual stress state is sought as a prerequisite for accurate life prediction of railroad rail affected by fatigue failure. This evolution includes manufacturing process (quenching and roller straightening), with inherent variations in material properties, track laying (neutral temperature and buckling risk), application of live loads (wheel wandering and wear), and maintenance (grinding).

References

[1] Cannon D.F., Edel K.-O., Grassie S.L., Sawley K., *Rail defects: an overview*, Fatigue Fract. Engng Mater. Struct., 2003, Vol. 26, 865–887.

[2] Cecot W., Orkisz J., *Prediction of Actual Residual Stresses Resulting from Cyclic Loading in Kinematic Hardening Material*, Proc. of the International Conference COMPLAS V, Barcelona 1997, 1879–1891.

[3] Crisfield M.A., *Non-linear Finite Element Analysis of Solids and Structures*, Wiley&Sons, 1994.

[4] Dang Van K., Maitournam M.H., Prasil B., *Elastoplastic analysis of repeated moving contact. Application to railways damage phenomena*, Wear, 1996, Vol. 196, 77–81.

[5] Forsythe G.E., Wasow W.R., *Finite Difference Methods for Partial Differential Equations*, Wiley, New York 1960.

[6] Groom J.J., *Determination of Residual Stresses in Rails, Batelle Columbus Laboratories*, Rpt. no. DOT/FRA/ORD-83-05, Columbus 1983.

[7] Jensen P.S., *Finite Difference techniques for variable grids*, Computers and Structures, 1972, Vol. 2, 17–29.

[8] Liszka T., Orkisz J., *The finite Difference at Arbitrary Irregular grids and its applications in applied mechanics*, Computers and Structures, 1980, Vol. 11, 109–121.

[9] Lo K.H., Mummery P., Buttle D.J., *Characterisation of residual principal stresses and their implications on failure of railway wheels*, Engng Failure Analysis, 2010, Vol. 17, 1273–1284.

[10] Magiera J., Orkisz J., Karmowski W., *Reconstruction of residual stresses in railroad rails from measurements made on vertical and oblique slices*, Wear, 1996, Vol. 191, 78–89.

[11] Marchenko H.P., *Influence of residual stresses on the stress intensity factors for a surface cracking the rail head*, Materials Science, 2010, Vol. 46, 64–69.

[12] Martin J.B., *Plasticity – fundamentals and general results*, The MIT Press Publ., 1975.

[13] Milewski S., Orkisz J., *Improvements in the global a-posteriori error estimation of the FEM and MFDM solutions*, Computing and Informatics, 2011, Vol. 30, 639–653.
[14] Orkisz J., Orringer O., Hołowiński M., Pazdanowski M., Cecot W., *Discrete Analysis of Actual Residual Stresses Resulting from Cyclic Loadings*, Computer and Structures, 1990, Vol. 35, 397–412.
[15] Orkisz J., Pazdanowski M., *On a new Feasible Directions solution approach in constrained optimization*, [in:] *The Finite Element Method in the 1990s*, Springer Verlag, 1991, 621–632.
[16] Orringer O., Tang Y.H., Gordon J.E., Morris J.M., Perlman A.B., *Crack propagation life of detail fractures in rail*, US DOT Final Rpt., DOT-TSC-FRA-88-1, Cambridge, MA 1988.
[17] Pazdanowski M., *On estimation of residual stresses in rails using shake-down based method, Archives of Transport*, 2010, Vol. 22, 319–336.
[18] Pazdanowski M., *Prediction of Residual Stresses in Railroad Rails by the Constrained Complementary Energy Minimization Shake-Down Method*, Final Rpt. to the US DOT, FRA, Washington DC, to be published.
[19] Ringsberg J.W., Josefson B.L., *Finite element analyses of rolling contact fatigue crack initiation in railheads*, J. Rail Rapid Transit, 2001, Vol. 215, 243–259.
[20] Ringsberg J.W., Lindback T., *Rolling contact fatigue analysis of rails including numerical simulations of the rail manufacturing process and repeated wheel-rail contact loads*, Int. J. of Fatigue, 2003, Vol. 25, 547–558.
[21] Sasaki T. et al., *Measurement of residual stresses in rails by neutron diffraction*, Wear, 2008, Vol. 265, 1402–1407.
[22] Schlenzer G., Fischer F.D., *Residual stress formation during the roller straightening of railway rails*, Int. J. of Mechanical Sciences, 2001, Vol. 43, 2281–2295.
[23] Skyttebol A., Josefson B.L., Rinsberg J.W., *Fatigue crack growth in a welded rail under the influence of residual stresses*, Engng Fracture Mechanics, 2005, Vol. 72, 271–285.
[24] Smith R.A., *Fatigue in transport. Problems, solutions and future threats*, Trans. IChemE: Part B, 1998, Vol. 76, 217–23.
[25] Steel R.K. et al., *Catastrophic Web Cracking of Railroad Rail: A Discussion of the Unanswered Questions*, Association of American Railroads, 1990.
[26] Telliskivi T., Olofsson U., *Wheel-rail wear simulation*, Wear, 2004, Vol. 257, 1145–1153.
[27] *The Derailment at Hatfield: A Final Report by the Independent Investigation Board (July 2006)*, UK. Office of Rail Regulation (ORR).
[28] Wang Y.Y., Chiang F.P., *Experimental study of three-dimensional residual stresses in rails by Moire interferometry and dissecting methods*, Optics and Lasers in Engng, 1996, Vol. 27, 89–100.
[29] Wrobel L.C., Aliabadi M.H., *The Boundary Element Method*, Wiley&Sons, 2002.
[30] Zerbst U., Lunden R., Edel K.-O., Smith R.A., *Introduction to the damage tolerance behavior of railway rails – a review*, Engng Fracture Mechanics, 2009, Vol. 76, 2563–2601.